

Seeking potential anticonvulsant agents that target GABA_A receptors using experimental and theoretical procedures

Margarita Virginia Saavedra-Vélez · José Correa-Basurto · Myrna H. Matus ·
Eloy Gasca-Pérez · Martiniano Bello · Roberto Cuevas-Hernández ·
Rosa Virginia García-Rodríguez · José Trujillo-Ferrara · Fernando Rafael Ramos-Morales

Received: 1 July 2014 / Accepted: 27 September 2014 / Published online: 9 October 2014
© Springer International Publishing Switzerland 2014

Abstract The aim of this study was to identify compounds that possess anticonvulsant activity by using a pentylenetetrazol (PTZ)-induced seizure model. Theoretical studies of a set of ligands, explored the binding affinities of the ligands for the GABA_A receptor (GABA_AR), including some benzodiazepines. The ligands satisfy the Lipinski rules and contain a pharmacophore core that has been previously reported to be a GABA_AR activator. To select the ligands with the best physicochemical properties, all of the compounds were analyzed by quantum mechanics and the energies of the highest occupied molecular orbital and lowest unoccupied molecular orbital were determined. Docking calculations between the ligands and the GABA_AR were used to identify the complexes with the

highest Gibbs binding energies. The identified compound D1 (dibenzo(*b,f*)(1,4)diazocine-6,11(5H,12H)-dione) was synthesized, experimentally tested, and the GABA_AR–D1 complex was submitted to 12-ns-long molecular dynamics (MD) simulations to corroborate the binding conformation obtained by docking techniques. MD simulations were also used to analyze the decomposition of the Gibbs binding energy of the residues involved in the stabilization of the complex. To validate our theoretical results, molecular docking and MD simulations were also performed for three reference compounds that are currently in commercial use: clonazepam (CLZ), zolpidem and eszopiclone. The theoretical results show that the GABA_AR–D1, and GABA_AR–CLZ complexes bind to the benzodiazepine binding site, share a similar map of binding residues, and have similar Gibbs binding energies and entropic components. Experimental studies using a PTZ-induced seizure model showed that D1 possesses similar activity to CLZ, which corroborates the predicted binding free energy identified by theoretical calculations.

Electronic supplementary material The online version of this article (doi:10.1007/s10822-014-9798-z) contains supplementary material, which is available to authorized users.

M. V. Saavedra-Vélez · J. Correa-Basurto (✉) · M. Bello ·
R. Cuevas-Hernández · J. Trujillo-Ferrara
Laboratorio de Modelado Molecular, Bioinformática y Diseño
de Fármacos de la Escuela Superior de Medicina IPN,
11340 Mexico City, Mexico
e-mail: corrjose@gmail.com

M. V. Saavedra-Vélez
Instituto de Neuroetología, Universidad Veracruzana, Xalapa,
Veracruz, Mexico

M. H. Matus · E. Gasca-Pérez · R. V. García-Rodríguez ·
F. R. Ramos-Morales (✉)
Unidad de Servicios de Apoyo en Resolución Analítica,
Universidad Veracruzana, A. P. 575, Xalapa, Veracruz, Mexico
e-mail: cambioramos@hotmail.com

E. Gasca-Pérez
Centro de Investigaciones Cerebrales, Universidad Veracruzana,
Xalapa, Veracruz, Mexico

Keywords Docking · GABA_AR · Synthesis · MD simulations

Introduction

Gamma-amino butyric acid (GABA) is the major inhibitory neurotransmitter in the mammalian brain, and its effects are mediated through two types of receptors: ionotropic (GABA_AR and GABA_CR) and metabotropic (GABA_BR) [1]. The GABA_AR is a member of the Cys-loop family of pentameric ligand-gated ion channels (pLGICs), and its structural topology consists of pentameric combinations of 19 different (α 1-6, β 1-3, γ 1-3, δ , ϵ , π , θ , ρ 1-3) polypeptide

subunits arranged around a central pore constituting an ion channel [2]. Most native GABA_ARs have two α subunits, two β subunits, and one γ or δ subunit and are usually type $2\alpha_12\beta_2\gamma_2$. GABA_AR can be bound by benzodiazepines (BZDs) as well as other structurally diverse ligands [3] that bind to the benzodiazepine (BZD) binding site and act as allosteric modulators to enhance GABA_AR activity [4]. The BZD binding site is located on the extracellular surface of GABA_AR and consists of several residues situated in at least six unconnected regions (loops A–F) at the α/γ interface [5]. BZD can be used to treat several disorders through its anxiolytic, hypnotic, anticonvulsant, and antispasmodic effects [6]. Most BZDs display sedative-hypnotic, muscle relaxant and amnesic properties due to the extrasynaptic location of GABA_ARs [7]. BZD analogs have broad biological applications and have been used as platelet aggregation and cyclooxygenase inhibitors as well as antihypertensive and anxiolytic agents. Previous studies have demonstrated the biological potential of BZD analogs for use as antidepressive agents that act on the central nervous system (CNS) [8–10].

The three-dimensional high-resolution (3D) structures of the subtypes of the GABA_ARs are currently unknown, but considerable information is known about the GABA_AR 3D structure based on computational modeling [11–13]. Additionally, several residues involved in stabilizing the ligands in the BZD binding site have been identified by mutagenesis studies [11–14]. Docking and molecular dynamics (MD) simulations have been used to obtain useful structural information for drug design [15, 16]. Furthermore, molecular analysis is important for gaining additional structural insights to identify promising drug candidates with greater bioavailability (i.e., complying with Lipinski rules) and lower toxicity [17]. Target recognition can be partially explained by several physicochemical properties of the ligands that can be determined by quantum chemistry, including the energies of the highest occupied molecular orbital (HOMO) and the lowest unoccupied molecular orbital (LUMO) [18, 19].

In this study, firstly a series of benzazepines (BZPs), benzodiazocines (BZCs) and BZDs were optimized using density functional theory (DFT) calculations. Then, these optimized structures were coupled to the GABA_AR through molecular docking to select the complexes with the best binding free energy values. Derived from these analyses, it was possible to observe a group of compounds that exhibited high Gibbs binding energies towards the GABA_AR. Among these compounds, compound D1 (dibenzo(*b,f*)(1,4)diazocine-6,11(5H,12H)-dione) not only showed a high Gibbs binding energy, and good ADME (absorption, distribution, metabolism, and excretion) properties (according to Lipinski rules), but also allowed to be synthesized. Then, to get further insight about the stability of D1 compound in the BZD

binding. Compound D1, together with clonazepam (CLZ), zolpidem (ZOP), and eszopiclone (ESZ), which are commercially used BZD (CLZ) or BZD analogs (ZOP and ESZ) with anticonvulsant activity were submitted to 12-ns-long MD simulation combined with the molecular mechanics generalized born surface area (MM-GBSA) method to calculate the absolute binding free energies, which were further decomposed on a per residue basis [20, 21]. The theoretical results show that the four compounds achieved stable ligand conformations in the BZD binding site. The GABA_AR–D1, GABA_AR–CLZ, and GABA_AR–ZOP complexes showed similar binding free energies, but only compounds D1 and CLZ were stabilized by similar residues in the BZD binding site. The efficacy of the theoretically designed and synthesized compound, D1 was determined as an anticonvulsant agent by using a pentylenetetrazol (PTZ)-induced seizure model. The anticonvulsant test showed that D1 possesses similar activity to CLZ, which although is not a first-line drug for the treatment of epilepsy, it is used when carbamazepine or valproic acid are not effective in helping patients [22, 23], and corroborated the predicted binding free energy identified by theoretical calculations. Furthermore, in this contribution we evidence a new potential compounds that could be one pharmaceutical option to target GABA_AR as anticonvulsive agent, which is easy to be synthesized.

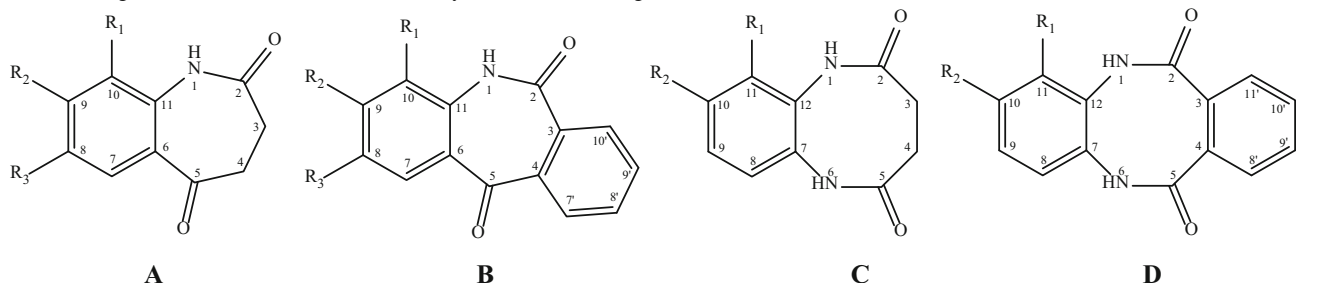
Computational methods

Optimization of ligands and calculation of frontier molecular orbitals

The structures of the various ligands were initially optimized by a PM3 [24, 25] semi-empirical method and improved by the B3LYP/DGDZVP2 [26–28] level of calculation. For the latter calculation, the frontier molecular orbitals (HOMO and LUMO) were visualized by applying an isovalue of 0.05 au. All calculations were carried out in Gaussian 03 [29].

GABA_AR ligand selections

It is widely known that GABA_AR recognizes the BZP pharmacophore. We used this core scaffold to design a drug by modifying several groups to increase the ligand affinity toward the GABA_AR (Table 1). The selected ligands were geometrically optimized using Gaussian 03 with the PM3 semi-empirical method, and improved by the DFT level of calculation (B3LYP/DZVP2). The optimized structures were loaded into AutoDockTools 1.5.2 [30] to prepare the input files for docking studies.

Table 1 Ligands tested by docking simulations on the GABA_AR


R1	R2	R3	Compound	ΔG	Compound	ΔG	Compound	ΔG	Compound	ΔG
H	H	H	A1	-5.85	B1	-8.13	C1	-6.65	D1	-7.60
NO ₂	H	H	A2	-6.66	B2	-8.75	C2	-7.62	D2	0.18
CH ₃	H	H	A3	-5.69	B3	-8.08	C3	-6.85	D3	0.00
OCH ₃	H	H	A4	-5.32	B4	-7.94	C4	-6.85	D4	0.23
F	H	H	A5	-5.82	B5	-7.94	C5	-6.51	D5	-0.68
Cl	H	H	A6	-5.92	B6	-8.06	C6	-6.76	D6	-0.68
OH	H	H	A7	-6.25	B7	-8.25	C7	-6.90	D7	0.30
CO ₂	H	H	A8	-6.85	B8	-8.54	C8	-7.56	D8	-0.07
NH ₂	H	H	A9	-5.53	B9	-7.72	C9	-7.38	D9	0.30
H	NO ₂	H	A10	-5.49	B10	-8.81	C10	-7.81	D10	0.00
H	CH ₃	H	A11	-7.02	B11	-8.83	C11	-7.13	D11	0.00
H	OCH ₃	H	A12	-5.38	B12	-8.29	C12	-6.93	D12	0.29
H	F	H	A13	-5.56	B13	-7.86	C13	-6.52	D13	-0.68
H	Cl	H	A14	-6.69	B14	-7.97	C14	-7.19	D14	-1.36
H	OH	H	A15	-5.12	B15	-7.92	C15	-7.25	D15	0.30
H	CO ₂	H	A16	-6.24	B16	-8.79	C16	-7.04	D16	0.30
H	NH ₂	H	A17	-5.67	B17	-8.00	C17	-7.15	D17	0.30
H	H	NO ₂	A18	-5.75	B18	-8.65	C18	-7.81	D18	0.30
H	H	CH ₃	A19	-5.82	B19	-8.82	C19	-6.77	D19	0.00
H	H	OCH ₃	A20	-5.82	B20	-9.01	C20	-7.06	D20	0.28
H	H	F	A21	-5.71	B21	-8.18	C21	-6.53	D21	-0.68
H	H	Cl	A22	-6.54	B22	-7.06	C22	-6.99	D22	-1.36
H	H	OH	A23	-5.84	B23	-8.69	C23	-7.25	D23	0.30
H	H	CO ₂	A24	-6.65	B24	-8.43	C24	-7.05	D24	0.30
H	H	NH ₂	A25	-5.57	B25	-8.64	C25	-7.11	D25	0.30
			ZOP	-9.55	CLZ	-8.61	ESZ	-8.65	DZP	-9.02

Gibbs energy values (in kcal/mol) corresponding to the BZD binding site using AutoDock 4.0.1

ZOP zolpidem, ESZ eszopiclone, CLZ clonazepam, DZP diazepam

Docking simulations

To identify and analyze the corresponding binding sites, the tested ligands were docked into the GABA_AR structure reported by Muroi et al. [13]. The Muroi et al. structure only includes the α_1 (UniProt ID: P14867) and γ_2 (UniProt ID: P18507) subunits, but contains the classical BZD binding pocket in a cleft between the α_1 and γ_2 subunits. To prepare the GABA_AR for docking, hydrogen atoms were added using the PSFGEN program included in visual molecular dynamics (VMD) 1.8 [31]. Then the entire

receptor was minimized with 2,000 steps using the CHARMM27 force field [32] and implemented in nano-scale molecular dynamics (NAMD) 2.6 [33]. The ligands were geometrically optimized using Gaussian 03, as described above. Next, the potentially flexible bonds were identified, and the partial atomic charges of the ligands (Gasteiger–Marsili formalism) were calculated using AutoDockTools 1.5.2. For the receptor, polar hydrogens were added and then Kollman charges for all atoms were computed to evaluate hydrogen-bonding interactions. All of the other parameters were kept at their default settings.

The receptor exploration and binding site definitions were prepared using a GRID-based approach [34], with a $126 \times 126 \times 126$ Å point grid centered on the receptor with 0.375 Å spacing. All of the simulations used the hybrid Lamarckian Genetic Algorithm [30], with an initial randomly placed population of 100 individuals and 1×10^7 evaluations. Docked orientations within a root-mean square deviation (RMSD) of 0.5 Å were clustered together. The lowest Gibbs energy cluster returned for each compound that was docked into the GABA_AR structure was used for further analysis. The interactions of the ligands with GABA_AR were visualized using AutoDock-Tools 1.5.2 [30].

Molecular dynamics simulations

Twelve ns-long MD simulations combined with the MM-GBSA approach were used to make a more detailed binding free energy calculation and to obtain more reliable information about the binding free energies of the docked complexes. These simulations and the analysis of their trajectories were performed in AMBER 12 [35] using an FF99SB force field [36]. Complexes were constructed using the Leap module, minimized by the Sander module, and MD simulations were performed using the “pmemd” module. The force field parameters for the ligands were generated with the antechamber module, based on the general AMBER force field (GAFF) [37], followed by optimization of ligands at the AM1-BCC [38]. Chloride ions were added to the most electropositive areas around the complexes to ensure the overall electroneutrality of the system at pH 7. The protein–ligand complexes were then solvated in a rectangular-shaped box of TIP3P water molecules [39] with a margin of 12.0 Å in each direction from the solution. The systems were equilibrated by carrying out minimization through 1,000 steps of steepest descent minimization followed by 1,000 steps of conjugate gradient minimization, 100 picoseconds (ps) of heating and 100 ps of density equilibration with weak restraints on the complex followed by 300 ps of constant pressure equilibration at 300 K, using the SHAKE algorithm [40] on hydrogen atoms, a time step of 2 femtoseconds (fs) and langevin dynamics for temperature control. The equilibration run was followed by a 12 ns MD run without position restraints under periodic boundary conditions. The particle mesh Ewald algorithm was applied to calculate long-range electrostatic interactions [41]. The cut-off distance for the long-range electrostatic and van der Waals (vdW) energy terms was set at 8.0 Å. The time step of the MD simulations was set to 2.0 fs, and the SHAKE algorithm [40] was used to constrain bond lengths at their equilibrium values. Temperature and pressure were maintained using the weak-coupling algorithm [42] with coupling constants τ_T and τ_P of 1.0 and 0.2 ps, respectively (at 300 K and 1 atm). Coordinates were

saved for analysis every 1 ps. Analysis of the trajectories was performed over the simulation time where the system reached equilibrium using AMBER analysis tools [35] and PyMOL [43].

MM-GBSA calculations for Gibbs binding energy

The binding free energy was calculated using the MM-GBSA approach [20, 21] in the Amber 12 package [35], using a salt concentration of 0.1 M and the Born implicit solvent model $igb = 2$ [44]. We chose a total number of 700 snapshots taken at regular intervals of 10 ps during the last 7 ns of the MD trajectory. The relative binding free energy (ΔG_{mmgsa}) of each complex can be conceptually summarized as:

$$\Delta G_{mmgsa} = G^{complex} - G^{receptor} - G^{ligand}$$

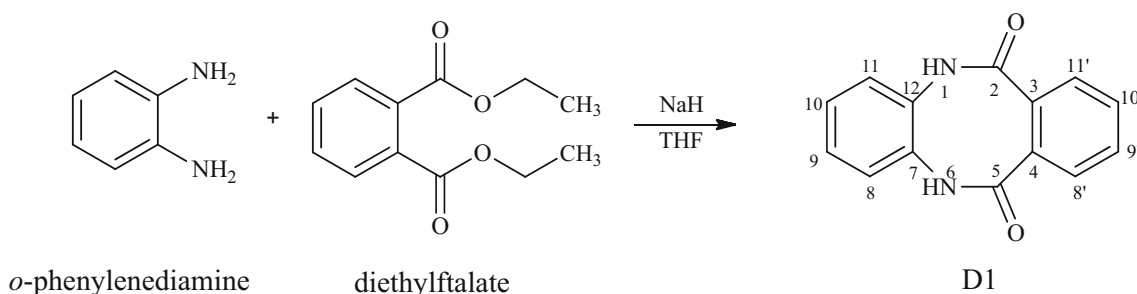
$$\Delta G_{bind} = \Delta E_{MM} + \Delta G_{GB} + \Delta G_{SA} - T\Delta S$$

where ΔE_{MM} is the total molecular mechanics energy of molecular system in the gas phase, including the van der Waals (ΔE_{vdw}) and electrostatic (ΔE_{ele}) interaction energies. ΔG_{GB} and ΔG_{SA} are electrostatic and nonpolar contributions to desolvation upon ligand binding, respectively. $-T\Delta S$ refers to the entropy contribution emerging from changes in the degrees of freedom of the solute molecules, which was used here to obtain ΔG_{bind} ; therefore, our values reported for the MMGBSA calculations can be called absolute binding free energies (ΔG_{bind}).

The entropy was estimated using a normal mode analysis of 25 snapshots with the MMPBSA.py module implemented in Amber Analysis Tools [35]. Because this calculation is memory intensive, we could not apply it to the entire system. Instead, we utilized an approach reported elsewhere where only the residues with any atom within 8 Å of the ligand in the last snapshot (truncated system) are considered when performing the entropy calculation [45]. To this aim, an 8 Å sphere around the ligand was cut out from each of the 25 MD snapshot for each ligand–protein complex. Each of those structures was minimized using a distance-dependent dielectric constant of $\epsilon = 4r$, to account for solvent screening, and its entropy was calculated using the normal mode analysis. After minimization, the entropy estimations were averaged over the 25 snapshots and quoted the standard error of the mean as a measure of the variance. The contribution of each residue to the Gibbs binding energy was determined by Gibbs energy decomposition (Fig. 3).

Synthesis

Compound D1 was synthesized as follows. To a mixture of 3.24 g (0.03 mol) of *o*-phenylenediamine and 6.66 g



Scheme 1 Synthesis of compound D1

(0.03 mol) of diethyl phthalate in 60 mL of dry tetrahydrofuran in a flask was added 2.9 g (0.06 mol) of a 60 % oil dispersion of sodium hydride (Aldrich). The reaction mixture was stirred at room temperature until a vigorous reaction started; then it was cooled on ice and continuously stirred for 12 h, followed by gentle stirring and raised to room temperature. The final reaction mixture was diluted with 50 mL of distilled water that was added drop wise, and acidified with a 50 % HCl aqueous solution. A white solid precipitate was filtered, washed three times with 25 mL of a 1:1 mixture of ethanol and benzene, and recrystallized in dimethylformamide HPLC grade (Tedia). The crystals obtained were dried at 80 °C for 12 h. The reaction (Scheme 1) agrees with other reports of structurally related compounds [46, 47]. The chemical characterization data is showed and discussed in the later section.

Biological evaluation

Animals

Male Wistar rats ($n = 36$) weighing 250–350 g were housed in plastic cages (six per cage) containing wood chip bedding with available food and water ad libitum. Cages were maintained in a room with a light–dark cycle (12/12 h, lights on at 8 am). Animals were manipulated once per day over a 2-week period before testing, to accustom them to the protocol. Manipulation of rats was guided by the Society for Neuroscience Policy on the Use of Animals in Neuroscience Research from UV, Mexico.

Anticonvulsant test

Rats were randomly distributed into six groups ($n = 6$): Group V (propylene glycol, pH 3.5, with acetic acid as a vehicle), Group CLZ (CLZ 5 mg/kg), and four groups with different doses of the D1 compound (1.25, 2.5, 5 and 7.5 mg/kg of body weight). We did not use ZOP and EZP in this experimental phase because these drugs do not have anticonvulsant activity.

Each rat was orally administered 1.0 mL/kg of each solution. Animals were placed in individual acrylic cages. 2 h later, PTZ (50 mg/kg i.p. in 0.9 % NaCl solution) was administered to induce tonic–clonic seizures as described elsewhere [48–50]. During the 1,800 s immediately after PTZ administration, seizure latency (time from PTZ administration to the onset of the seizure), seizure duration, and recovery time were recorded. 24 h after the test, the animals were euthanized with pentobarbital (overdose, i.p.).

Statistical analysis

In the first analysis, data were analyzed with the Fisher exact test to determine if there were differences between groups (Table 2). Then, because the data had a *Poisson* distribution, the response variables (seizure latency, seizure duration, and recovery time) were evaluated by non-parametric one-way ANOVA using χ^2 values. This statistical procedure is used to find differences between groups when data do not have a normal distribution. A result was considered statistically significant when $p < 0.05$.

Results and discussion

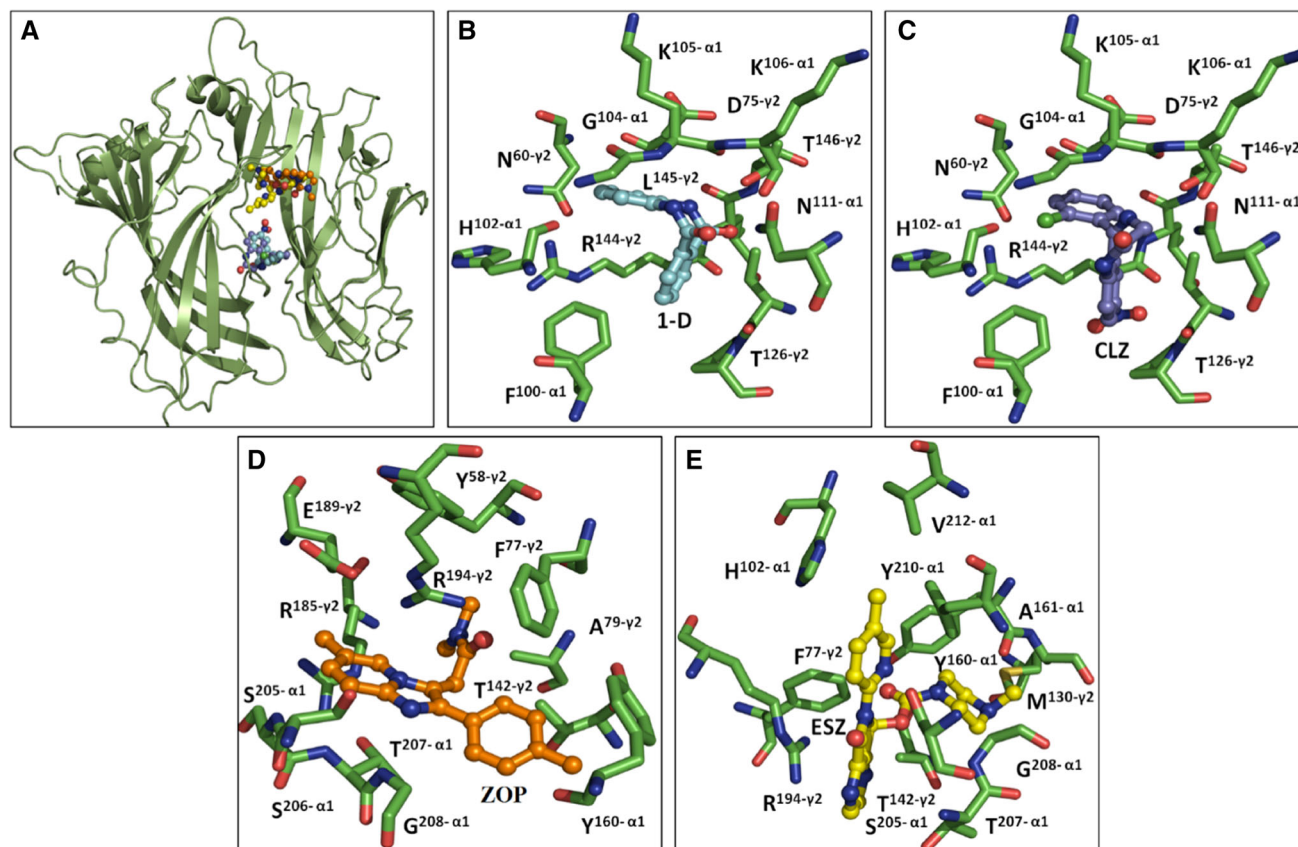
Docking studies

The chemical and physical properties of both the receptor and the ligand are important in the ligand recognition process. It is known that ligand properties such as frontier orbitals and stable conformers are related to biological activity [18, 19]. Therefore, the inclusion of several ligands in our analysis allowed for the selection of ligands with the best physicochemical properties (agreement with the Lipinski rules) and the most stable conformers.

A clear example of a stable conformer is given in the results. Structural ligand energy minimization showed that the A1 structure had two stable conformers with similar energies, whereas B1, C1, and D1 only had one conformer each. Starting from A1–D1 (Table 1), the molecules were substituted and re-optimized using the PM3 method,

Table 2 Number of animals that responded per treatment (Fisher's exact test)

Response/ treatment	V	1.25 (mg/ kg)	2.50 (mg/kg)	5.00 (mg/kg)	7.50 (mg/ kg)	CLZ
With seizure	5	5	1	2	6	1
Without seizure	1	1	5	4	0	5
Fisher's test	NS	NS	$p < 0.01$ versus V	$p < 0.01$ versus V	NS	$p < 0.01$ versus V

NS not significant ($p > 0.05$)**Fig. 1** Docking of the GABA_AR–D1, GABA_AR–CLZ, GABA_AR–ZOP, and GABA_AR–ESZ optimized complexes. **a** D1 (cyan), CLZ (violet), ZOP (orange), and ESZ (yellow) forming complexes with

resulting in 100 molecules in total. After the minimum energy optimization of the ligand structures, we performed docking calculations between the ligands and the optimized structure of the GABA_AR. By comparing the Gibbs free energy (ΔG) values and the dissociation constant (K_d), we could determine whether a given ligand exhibited affinity for and stability in the receptor binding site. Additionally, to validate our theoretical results, we performed docking calculations between the GABA_AR and three currently used commercial drugs, CLZ, ZOP, and ESZ as comparative models.

The results show that D1 and CLZ bind deeper in the BZD binding pocket than the two BZD analogs (Fig. 1a). In fact, the two BZDs were stabilized by the same type of residues

GABA_AR and in close proximity to the reported BZD binding site. **b** D1, **c** CLZ, **d** ZOP, and **e** ESZ establishing non-covalent interactions with residues belonging to the BZD binding site

(F^{100-α1}, H^{102-α1}, G^{104-α1}, K^{105-α1}, K^{106-α1}, N^{111-α1}, N^{60-γ2}, D^{75-γ2}, T^{126-γ2}, T^{146-γ2}, R^{144-γ2}, and L^{145-γ2}) through hydrophobic interactions corresponding to either the backbone or the side chain atoms (Fig. 1b, c). The two BZD analogs interacted with a large number of aromatic moieties (Fig. 1d, e) and interact with several residues (Y^{160-α1}, S^{205-α1}, T^{207-α1}, G^{208-α1}, F^{77-γ2}, T^{142-γ2}, and R^{194-γ2}). Furthermore, both docking complexes showed a map of interactions similar to those reported in other theoretical studies [14, 51]. Some residues were found to stabilize the BZD and BZD analogs, including F^{100-α1}, H^{102-α1}, Y^{160-α1}, V^{212-α1}, S^{205-α1}, S^{206-α1}, T^{207-α1}, Y^{210-α1}, F^{77-γ2}, A^{79-γ2}, and M^{130-γ2}, which are the same as those reported to be involved in the binding of BZD and BZD analogs [11–13]. Point mutations at some of these

residues affect the binding properties of the GABA_AR to the two BZD analogs [10].

Molecular dynamics simulations

Docking calculations are able to predict a map of interactions that are useful for predicting whether an interaction between a ligand and its binding site will be energetically favorable. MD simulations also have the advantage of using docking procedures to produce refined information about the interactions involved in the stabilization of a complex. Therefore, MD simulations were performed for the four aforementioned complexes obtained under docking procedures.

The conformational stabilities of the four systems in explicit solvent were examined by calculating the root-mean squared deviations (RMSD) of the receptor–ligand complex (the backbone with the energetically minimized ligand structure) during MD simulations lasting 12 ns. This analysis showed that the four complexes reached an RMSD plateau within the first 5 ns of simulation (supplementary material, Fig. 1S), with average RMSD values of 4.1 ± 0.22 , 3.87 ± 0.17 , 3.9 ± 0.20 , and 4.0 ± 0.14 Å for GABA_AR–D1, GABA_AR–CLZ, GABA_AR–ESZ, and GABA_AR–ZOP, respectively. Therefore, all subsequent analyses excluded the initial 5 ns period.

Interactional analysis and average properties

The GABA_AR–D1, GABA_AR–CLZ, and GABA_AR–ZOP average structures obtained through MD simulations showed only slight variations with respect to the complexes predicted by docking procedures. However, there was a notable difference between the GABA_AR–ESZ average structure and the complex obtained from docking procedures (Figs. 1e, 2h). The GABA_AR–D1 and GABA_AR–CLZ complexes shared a considerable number of residues in both the docked and average structure (Figs. 1b, c, 2b, d). Nevertheless, the maps of the interactions for the average structures were better optimized than those from the docking procedure. The nonpolar region of D1 and CLZ in both average structures shows interactions with three benzene aromatic rings (F^{100- α 1}, F^{101- α 1} and Y^{160- α 1}) that participate in important π – π interactions. However, this region in the docking complex showed only one interaction (F^{100- α 1}) (Figs. 1b, c, 2b, d). In addition, D1 and CLZ in the average structure formed a salt bridge with R^{144- γ 2}, whereas under docking procedures, R^{144- γ 2} only contributed to the stabilization of the ligand through non-polar contacts.

In an approximately similar mode, the GABA_AR–ZOP complex was stabilized by similar types of residues using both techniques, but with some differences in the binding

distribution. A cluster of aromatic residues was observed to stabilize ZOP, while a salt bridge with R^{194- γ 2} stabilized the polar atoms of ZOP (Figs. 1d, 2f).

The GABA_AR–ESZ complex showed the most notable difference between the two procedures, and interactions with only four residues were shared (Figs. 1e, 2h). In fact, Fig. 2g shows that ESZ rotates upon its axis, which favors interactions that are different from those observed for the docking complex. Overall, these results show that the MD simulation provided a better map of interactions for the GABA_AR–D1, GABA_AR–CLZ, and GABA_AR–ZOP complexes but not for the GABA_AR–ESZ complex.

Binding free energy calculation and energy decomposition

Binding free energies were calculated for 700 snapshots collected at regular intervals of 10 ps during the last 7 ns of MD simulations, and the results are listed in Table 3. This Table shows that the absolute binding free energy (ΔG_{bind}) was favorable for GABA_AR–D1, GABA_AR–CLZ, and GABA_AR–ZOP, and the non-polar interactions (ΔE_{npol}) were the driving forces for binding. The van der Waals interactions (ΔE_{vdw}) make major contributions to binding because they all have good hydrophobic contacts. Surprisingly, although the GABA_AR–ESZ complex had a favorable relative binding free energy (ΔG_{mngbsa}), this value was almost cancelled out by the entropic component, which gave an unfavorable ΔG_{bind} . The gas-phase electrostatic energies (ΔE_{ele}) show that, despite the fact that GABA_AR–D1, GABA_AR–CLZ, and GABA_AR–ZOP complexes have small negative ΔE_{ele} values, they all have unfavorable polar energies (ΔE_{polar}), creating an unfavorable contribution to the ΔG_{bind} . For the GABA_AR–ESZ complex, no favorable ΔE_{ele} values were observed. Overall, the positive ΔE_{polar} observed for the four complexes means that the ligands have stronger polar interactions with the solvent than with the receptor, and the entropic contribution was consistent for the four complexes. Upon complex formation, these systems decreased their degrees of freedom and had unfavorable entropy contributions to the Gibbs binding energy. However, the GABA_AR–ESZ complex showed the highest entropy value, which also contributed to its unfavorable ΔG_{bind} .

Energy decomposition enables us to observe the energetic contributions of each residue in the complex. Figure 3 depicts the key residues for binding and their total energy contributions (ΔG_{bind}). These Figures show that the GABA_AR–D1, GABA_AR–CLZ complexes are mainly stabilized by hydrophobic residues which, according to the structural analysis, are because of interactions with their side chain or backbone atoms (Fig. 2b, d). Total free energy contributions show that the F^{100- α 1}, F^{101- α 1}, V^{108- α 1},

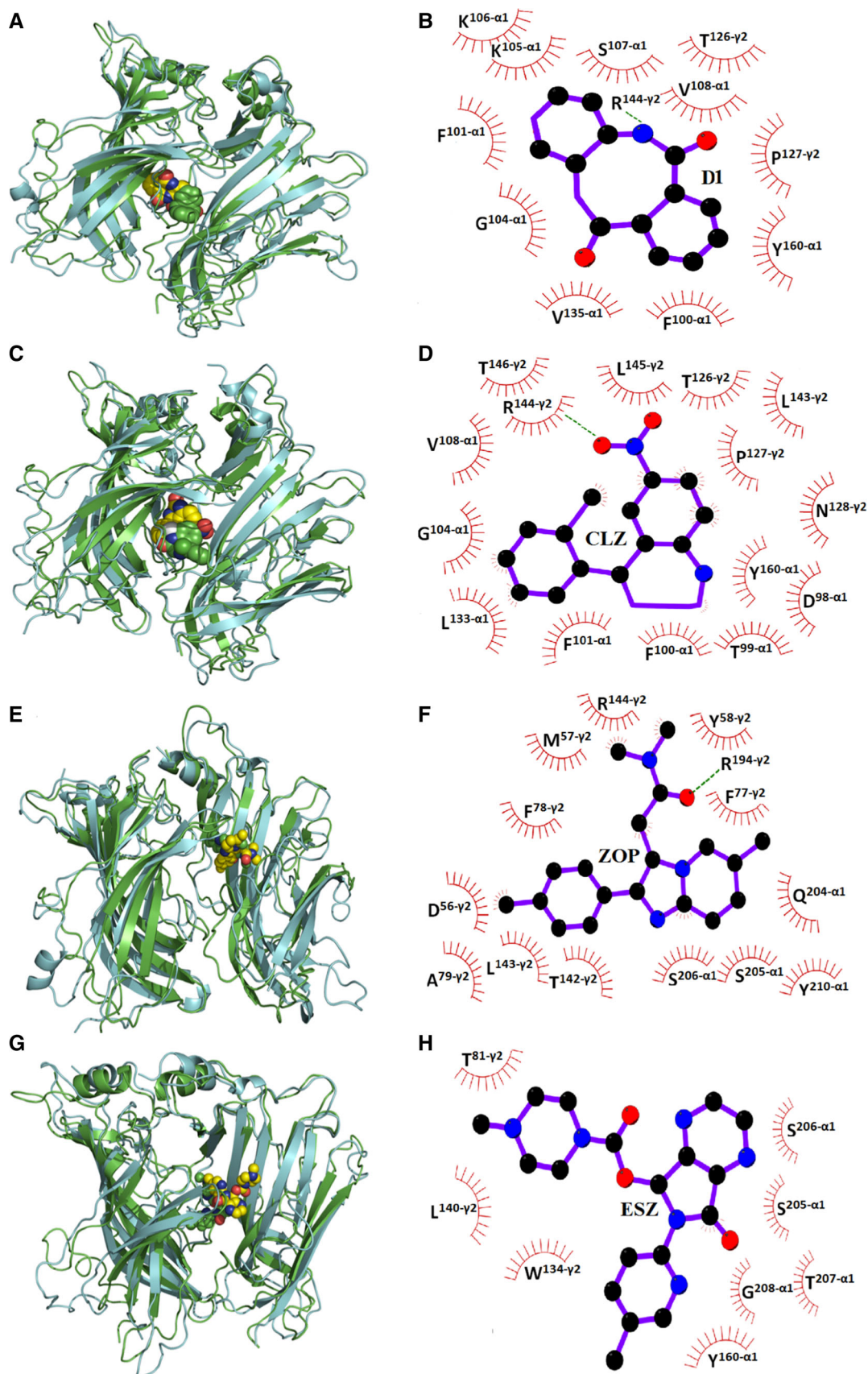


Fig. 2 Docking and average conformation complexes formed between GABA_AR and the four different compounds (D1, CLZ, ZMP, and ESZ). Docking (green) and average conformation (cyan) of the GABA_AR–D1 (a), GABA_AR–CLZ (c), GABA_AR–ZOP (e), and GABA_AR–ESZ complexes (g). Detailed interactions for the GABA_AR–D1 (b), GABA_AR–CLZ (d), GABA_AR–ZOP (f), and GABA_AR–ESZ (h) complexes. The residues in close proximity (≤ 0.5 nm) to the ligands and those that made important contributions to the Gibbs binding energy are depicted as schematic representations using LIGPLOT v.4.5.3 [62]

$Y^{160-\alpha 1}$, $T^{126-\gamma 2}$, $P^{127-\gamma 2}$, and $R^{144-\gamma 2}$ residues of GABA_AR have the greatest contributions to the binding energy, suggesting that these residues are important for ligand binding. However, while the types of residues stabilizing GABA_AR–D1 and GABA_AR–CLZ complexes share several ligand–receptor interactions, the residues responsible for binding are very different in the GABA_AR–ESZ and GABA_AR–ZOP complexes. Only $R^{144-\gamma 2}$ participated in the stabilization of the GABA_AR–D1, GABA_AR–CLZ, and GABA_AR–ZOP (Fig. 3) with a more significant energetic contribution for the formation of the GABA_AR–D1 and GABA_AR–CLZ complexes. According to this analysis, $F^{100-\alpha 1}$, $F^{101-\alpha 1}$, $V^{108-\alpha 1}$, $Y^{160-\alpha 1}$, $T^{126-\gamma 2}$, $P^{127-\gamma 2}$, and $R^{144-\gamma 2}$ were crucial for stabilizing the GABA_AR–D1 and GABA_AR–CLZ complexes (Fig. 3a, b), whereas stabilization of the GABA_AR–ZOP complex was mostly achieved by a salt bridge between the oxygen atom of ZOP and the side chain of R^{194-E} (Fig. 3c). The GABA_AR–ESZ complex had the lowest number of interactions but shared only a few interactions with GABA_AR–D1 and GABA_AR–CLZ ($Y^{160-\alpha 1}$) and GABA_AR–ZOP ($S^{205-\alpha 1}$ and $S^{206-\alpha 1}$), with $T^{207-\alpha 1}$ being the main contributor to the total energy change per residue in the GABA_AR–ESZ complex.

Lipinski's rule and toxicity properties

To provide an estimate about the pharmacokinetic properties of the set of compounds under study, several molecular properties were calculated, including partition coefficient, solubility coefficient, polar surface area, molecular weight, number of hydrogen bond acceptors, number of hydrogen bond donors, number of rotatable bonds, reproductive effects and any toxic, mutagenic, tumorigenic, or irritant properties (Table 4) using two web servers (<http://www.molinspiration.com/> and <http://www.organic-chemistry.org/prog/peo/>). These calculations can help to predict if the compounds will be able to reach the target receptor after either oral or intravenous administration.

In general, the chemical properties of all of the compounds seem to indicate that they are not outside the Lipinski rules (Table 4). It seems likely that D1 orally administered could reach the central nervous system according to our experimental assays. Docking studies made it possible to select a ligand with good affinity and ADME properties, which then was synthesized and tested biologically. Docking procedures with the capability of recognizing potential binding sites [52] showed that the ligand bound in close proximity to the reported BZD binding site. On the other hand, MD simulations made it possible to obtain a more optimized map of the interactions between D1 and the GABA_AR. MD showed that this ligand reaches $F^{100-\alpha 1}$ and $Y^{160-\alpha 1}$ through π – π interactions. According to our MM-GBSA analysis, these residues proved to be energetically important for stabilizing the ligand–receptor complex and were also found to be important for BZD recognition. In addition, another important non-covalent interaction is the π –cation with $R^{144-\gamma 2}$, which is a charged residue known to be one of the most important for ligand recognition [51].

The map of interactions involved in stabilizing the GABA_AR–ZOP complex agrees with those reported elsewhere through both theoretical calculations and experimental results. On the other hand, the GABA_AR–ESZ complex obtained through MD simulations disagrees with those reported elsewhere from using docking procedures. However, there is experimental evidence indicating that cyclopyrrolones can reach multiple BZD binding sites on the GABA_AR in concert and produce allosteric changes in ligand affinity at the remaining sites. This suggests that the structural requirements for ESZ are different from those for ZOP.

HOMO and LUMO analysis

The HOMO is the most likely site for an electrophilic attack, and the LUMO is the most likely site to undergo a nucleophilic attack. Of the four parent molecules designed

Table 3 Gibbs binding energy for the GABA_AR–ligand complexes (in kcal/mol)

System	ΔE_{vdw}	ΔE_{ele}	ΔG_{GB}	ΔG_{SA}	ΔE_{polar}	ΔE_{npol}	ΔG_{mmgbsa}	$-T\Delta S$	ΔG_{bind}
GABA _A R–D1	–38.92 (0.11)	–5.05 (0.12)	17.43 (0.07)	–3.70 (0.17)	+12.38	–42.62	–30.24 (0.10)	–15.36 (2.87)	–14.88
GABA _A R–CLZ	–38.11 (0.11)	–11.7 (0.12)	23.52 (0.07)	–4.83 (0.17)	+11.82	–42.94	–31.12 (0.10)	–13.80 (2.5)	–17.32
GABA _A R–ZOP	–36.2 (0.40)	–20.30 (0.53)	27.84 (0.54)	–5.90 (0.07)	+7.54	–42.1	–34.56 (0.45)	–17.10 (2.95)	–17.46
GABA _A R–ESZ	–26.0 (0.18)	205 (0.63)	–193 (0.54)	–5.37 (0.02)	+12.0	–31.37	–19.37 (0.17)	–20.76 (2.67)	+1.39

The polar (ΔE_{ele} + ΔG_{GB}) contributions (ΔE_{polar}) and the non-polar (ΔE_{vdw} + ΔG_{SA}) contributions (ΔE_{npol}). All the energies are averaged over several snapshots (see “Computational methods” section) and are in kcal/mol (\pm standard error of the mean)

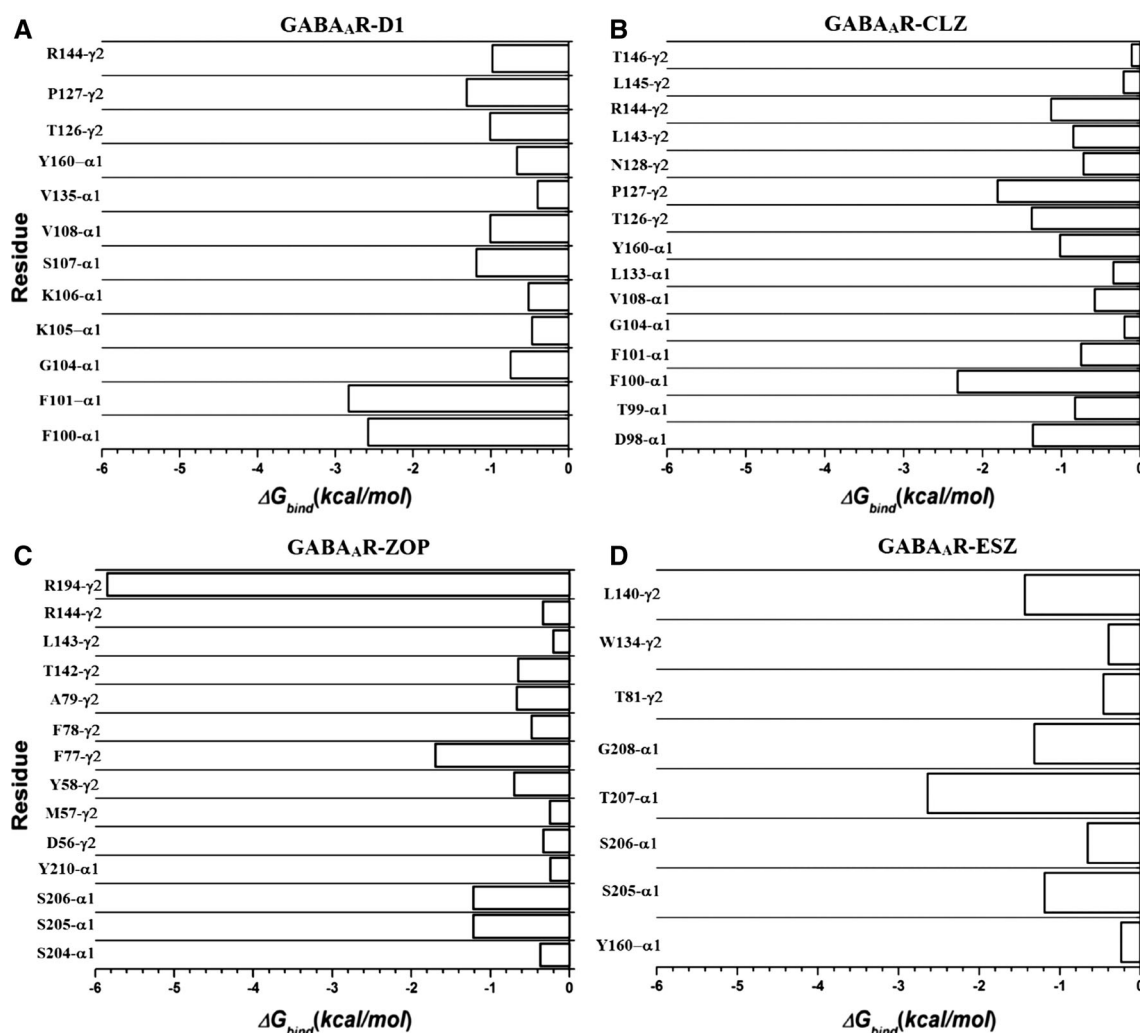


Fig. 3 Deconvolution of the total Gibbs binding energy (ΔG_{bind}) on a per-residue basis in four complexes: **a** GABA_AR-D1, **b** GABA_AR-CLZ), **c** GABA_AR-ZOP, and **d** GABA_AR-ESZ

in the present study (Table 1), two have a seven-membered ring (A1 and B1) and two have an eight-membered ring (C1 and D1). For these molecules, the HOMO can be found on the aromatic rings and the LUMO on the adjacent carbonyl group of A1, B1, and D1. C1 has both the HOMO and LUMO in the aromatic ring (Fig. 2S).

The results for the A series show that the $-\text{NO}_2$ group (A2, A10, A18) influences the LUMO distribution regardless of its position on the aromatic ring. In molecules with *meta*-substitution, all functional groups have important influence on the LUMO (A11–A17). In the B series, only B2, B10, B13, and B16 showed a substituent influence on LUMO delocalization. In the C ligand series, LUMO delocalization was observed mostly in the aromatic ring, except for C2, C8, C10, and C16 where the functional group attachment in the aromatic ring participates in the distribution of the frontier orbitals. In the D series, behavior similar to that in the B and C series is observed, as the $-\text{NO}_2$ and $-\text{CO}_2\text{H}$ (D10 and D16) substituents

contribute to the delocalization of the LUMO, but only in the *meta* position. Thus, the interaction with the GABA_AR most likely occurs by a π -cation interaction, which is an important force in biological recognition systems [53].

In A1 and B1, the HOMO is on the amide group and on the substituted aromatic ring (Fig. 2S). In contrast, C1 and D1 showed a slightly different distribution, where the HOMO is located in both the amide and aromatic moieties. In the A series, the HOMO distribution primarily depends on the contribution of the substituents, except for A3, A8, A10, A11, A16 and A19. An analog effect is shown in the B series for similar molecules with the same functional groups in the same positions on the aromatic ring (B3, B8, B10, B11, B16, and B19). For comparison, in the C and D series there is an influence by the electronegative functional groups. Thus, the structures with electrodonating groups (C3, C8, C11, and C16 and D3, D8, D11, and D16) do not affect the HOMO distribution in comparison to the parent compounds. This is because electronegative

Table 4 Molecular properties for the designed ligands

Ligand	Log P	Log S	PSA	MW	nON	nOHNH	nrotb	M	T	I	RE
A1	1.37	−2.73	49.169	175	3	1	0	1	1	1	1
A2	1.24	−3.19	91.993	220	6	1	1	0	1	1	1
A3	1.68	−3.07	46.169	189	3	1	0	1	1	1	1
A4	1.26	−2.75	55.403	205	4	1	1	1	1	1	1
A5	1.42	−3.04	46.169	193	3	1	0	1	1	1	1
A6	1.98	−3.46	46.169	209	3	1	0	1	1	1	1
A7	1.07	−2.43	66.397	191	4	2	0	1	1	1	1
A8	0.89	−2.74	83.468	219	5	2	1	1	1	1	1
A9	0.64	−2.8	72.192	190	4	3	0	0	1	1	1
A10	1.24	−3.19	91.993	220	6	1	1	1	1	1	1
A11	1.68	−3.07	46.169	189	3	1	0	1	1	1	1
A12	1.26	−2.75	55.403	205	4	1	1	1	1	1	1
A13	1.42	−3.04	46.169	193	3	1	0	1	1	1	1
A14	1.98	−3.46	46.169	209	3	1	0	1	1	1	1
A15	1.07	−2.43	66.397	191	4	2	0	1	1	1	1
A16	0.89	−2.74	83.468	219	5	2	1	1	1	1	1
A17	0.64	−2.8	72.192	190	4	3	0	1	1	0	1
A18	1.24	−3.19	91.993	220	6	1	1	1	1	1	1
A19	1.68	−3.07	46.169	189	3	1	0	1	1	1	1
A20	1.26	−2.75	55.403	205	4	1	1	0	1	1	1
A21	1.42	−3.04	46.169	193	3	1	0	1	1	1	1
A22	1.98	−3.46	46.169	209	3	1	0	1	1	1	1
A23	1.07	−2.46	66.397	191	4	2	0	1	1	1	1
A24	0.89	−2.74	83.468	219	5	2	1	1	1	1	1
A25	0.64	−2.8	72.192	190	4	3	0	1	1	0	1
B1	2.83	−4.14	49.933	223	3	1	0	1	1	1	1
B2	2.7	−4.6	95.757	268	6	1	1	0	1	1	1
B3	3.14	−4.49	49.933	237	3	1	0	1	1	1	1
B4	2.72	−4.16	59.167	253	4	1	1	1	1	1	1
B5	2.89	−4.46	49.933	241	3	1	0	1	1	1	1
B6	3.44	−4.88	49.933	257	3	1	0	1	1	1	1
B7	2.53	−3.85	70.161	239	4	2	0	1	1	1	1
B8	2.35	−4.16	87.232	267	5	2	1	1	1	1	1
B9	2.1	−4.22	75.956	238	4	3	0	0	1	1	1
B10	2.7	−4.46	95.757	268	6	1	1	1	1	1	1
B11	3.14	−4.49	49.933	237	3	1	0	1	1	1	1
B12	2.72	−4.16	59.167	253	4	1	1	1	1	1	1
B13	2.89	−4.46	49.933	241	3	1	0	1	1	1	1
B14	3.44	−4.88	49.933	257	3	1	0	1	1	1	1
B15	3.85	−3.85	70.161	239	4	2	0	1	1	1	1
B16	2.35	−4.16	87.232	267	5	2	1	1	1	1	1
B17	2.1	−4.22	75.956	238	4	3	0	1	1	0	1
B18	2.7	−4.6	95.757	268	6	1	1	1	1	1	1
B19	3.14	−4.49	49.933	237	3	1	0	1	1	1	1
B20	2.72	−4.16	59.167	253	4	1	1	0	1	1	1
B21	2.38	−4.46	49.933	241	3	1	0	1	1	1	1
B22	3.44	−4.88	49.933	257	3	1	0	1	1	1	1
B23	2.53	−3.85	70.161	239	4	2	0	1	1	1	1

Table 4 continued

Ligand	Log P	Log S	PSA	MW	nON	nOHNH	nrotb	M	T	I	RE
B24	2.35	−4.16	87.232	267	5	2	1	1	1	1	1
B25	2.1	−4.22	75.956	238	4	3	0	0	0	0	1
C1	1.25	−2.39	58.196	190	4	2	0	1	1	1	1
C2	1.12	−2.85	104.02	235	7	2	1	0	1	1	1
C3	1.56	−2.73	58.196	204	4	2	0	1	1	1	1
C4	1.14	−2.4	67.43	220	5	2	1	1	1	1	1
C5	1.3	−2.7	58.196	208	4	2	0	1	1	1	1
C6	1.86	−3.12	58.196	224	4	2	0	1	1	1	1
C7	0.95	−2.09	78.424	206	5	3	0	1	1	1	1
C8	0.77	−2.4	95.497	234	6	3	1	1	1	1	1
C9	0.52	−2.46	84.219	205	5	4	0	0	1	1	1
C10	1.12	−2.85	104.02	235	7	2	1	1	1	1	1
C11	1.56	−2.73	58.196	204	4	2	0	1	1	1	1
C12	1.14	−2.4	67.33	220	5	2	1	0	1	1	1
C13	1.3	−2.7	58.196	208	4	2	0	1	1	1	1
C14	1.86	−3.12	58.196	224	4	2	0	1	1	1	1
C15	0.95	−2.09	78.424	206	5	3	0	1	1	1	1
C16	0.77	−2.4	95.495	234	6	3	1	1	1	1	1
C17	0.52	−2.46	84.219	205	5	4	0	0	0	0	1
C18	1.12	−2.85	104.02	235	7	2	1	1	1	1	1
C19	1.56	−2.73	58.196	204	4	2	0	1	1	1	1
C20	1.14	−2.4	67.43	220	5	2	1	0	1	1	1
C21	1.13	−2.7	58.196	208	4	2	0	1	1	1	1
C22	1.86	−3.12	58.196	224	4	2	0	1	1	1	1
C23	0.95	−2.09	78.424	206	5	3	0	1	1	1	1
C24	0.77	−2.4	95.495	234	6	3	1	1	1	1	1
C25	0.52	−2.46	84.219	205	5	4	0	0	0	0	1
D1	2.67	−3.55	65.724	238	5	2	0	1	1	1	1
D2	2.54	−4.01	111.548	283	7	2	1	0	1	1	1
D3	2.98	−3.9	65.724	252	4	2	0	1	1	1	1
D4	2.56	−3.57	74.958	268	5	2	1	1	1	1	1
D5	2.73	−3.87	65.724	256	4	2	0	1	1	1	1
D6	3.28	−4.29	65.724	272	4	2	0	1	1	1	1
D7	2.37	−3.27	85.952	254	5	2	0	1	1	1	1
D8	2.19	−3.57	103.023	282	6	2	1	1	1	1	1
D9	1.95	−3.63	91.747	253	5	2	0	0	1	1	1
D10	2.54	−4.01	111.548	283	7	2	1	1	1	1	1
D11	2.98	−3.9	65.724	252	4	2	0	1	1	1	1
D12	2.56	−3.57	74.958	268	5	2	1	1	1	1	1
D13	2.73	−3.87	65.724	256	4	2	0	1	1	1	1
D14	3.28	−4.29	65.724	272	4	2	0	1	1	1	1
D15	2.37	−3.26	85.952	254	5	2	0	1	1	1	1
D16	2.19	−3.57	103.023	282	6	2	1	1	1	1	1
D17	1.95	−3.63	91.747	253	5	2	0	0	0	0	1
D18	2.54	−4.01	111.548	283	7	2	1	1	1	1	1
D19	2.98	−3.9	65.724	252	4	2	0	1	1	1	1
D20	2.56	−3.57	74.958	268	5	2	1	1	1	1	1
D21	3.28	−4.29	65.724	272	4	2	0	1	1	1	1

Table 4 continued

Ligand	Log P	Log S	PSA	MW	nON	nOHNH	nrotb	M	T	I	RE
D22	2.73	−3.87	65.724	256	4	2	0	1	1	1	1
D23	3.28	−4.29	85.952	272	5	2	0	1	1	1	1
D24	2.19	−3.57	103.023	282	6	2	1	1	1	1	1
D25	1.95	−3.63	91.747	253	5	2	0	0	0	0	1
ZOP	3.15	−5.03	37.616	307	4	0	3	0	0	0	0
ESZ	0.48	−1.74	90.71	391	9	0	3	1	1	1	1
CLZ	2.77	−5.16	87.286	316	6	1	2	0	0	0	0
BZD	2.73	−4.67	32.673	285	3	0	1	0	0	0	0

Toxic properties, *M* mutagenic, *T* tumorigenic, *I* irritant, and *RE* reproductive effective; for physicochemical properties, 1 = favorable and 0 = unfavorable, whereas for toxic properties 1 = non toxic, 0 = toxic

Log P partition coefficient, *Log S* solubility coefficient, *PSA* polar surface area, *MW* molecular weight, *nON* number of hydrogen bond acceptors, *nOHNH* number of hydrogen bond donors, *nrotb* number of rotatable bonds

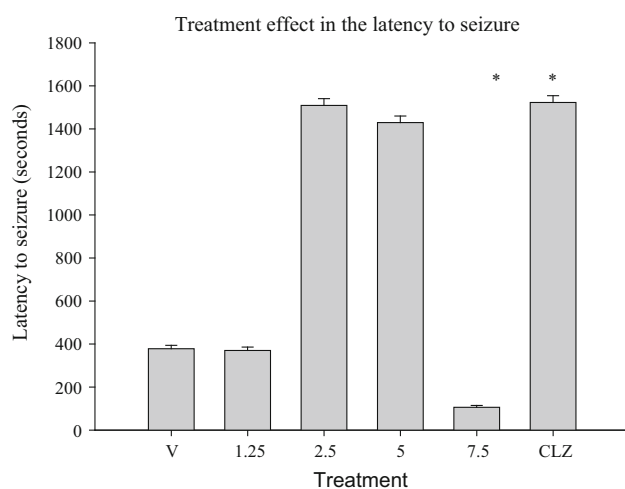


Fig. 4 Effect of D1 on the latency (in seconds) of the convulsions induced by PTZ in male rats. Each point represents the mean \pm CI for $n = 6$ rats per dose. *Significant effect compared with the V group (non-parametric one-way ANOVA, $p < 0.05$)

functional groups affect the nucleophilic attack of the amino acid residues on the GABA_AR binding site.

Finally, to validate our theoretical results we focused on performing the synthesis of one of the promissory compounds. Although the compound with the best affinity on GABA_AR was B24 (according to molecular modeling results), D1 compound was synthesized due to the fact that not only displayed very good ADME properties and exhibited good free energy values, but also was more straightforward to be synthesized.

Characterization of D1 compound

Dibenzo(*b,f*)(1,4)diazocine-6,11(5H,12H)-dione (D1): 60 %, m.p.: 301 °C; ^1H NMR (DMSO-*d*₆) δ 7.2 (dd, 4H, $J = 0.55$; $J = 4.66$), 7.3 (t, 2H), 7.4 (t, 2H, $J = 3.3$), 10.2 (s, 2H, N). ^{13}C

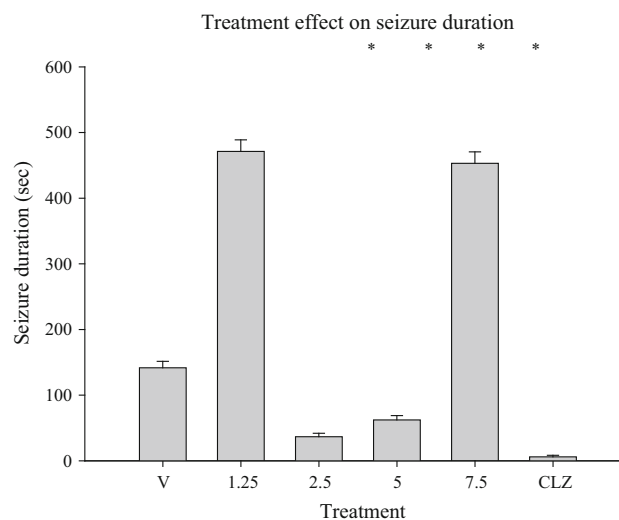


Fig. 5 Effect of D1 on the duration (in seconds) of the convulsions induced by PTZ in male rats. Each point represents the mean \pm CI for $n = 6$ rats per dose. *Significant effect compared with the V group (non-parametric one-way ANOVA, $p < 0.05$)

NMR (DMSO-*d*₆) δ 127.0 (s, C8, C11), 127.4 (s, C9, C10), 128.0 (s, C9', C10'), 130.7 (s, C8', C11'), 132.6 (s, C7, C12), 135.2 (s, C3, C4), 170.8 (s, C2, C5). MS-EI: 238.

Anticonvulsant evaluation

The Fisher exact test showed that only the CLZ and two D1 treatments (2.50 and 5.00 mg/kg) showed significant differences from the V group ($p < 0.01$) in the type of response and the number of animals that responded to treatment (Table 2). Data obtained from the non-parametric one-way ANOVA analysis showed that these three treatment groups had a longer seizure latency than both group V and the D1 treatments using 1.25 and 5.00 mg/kg

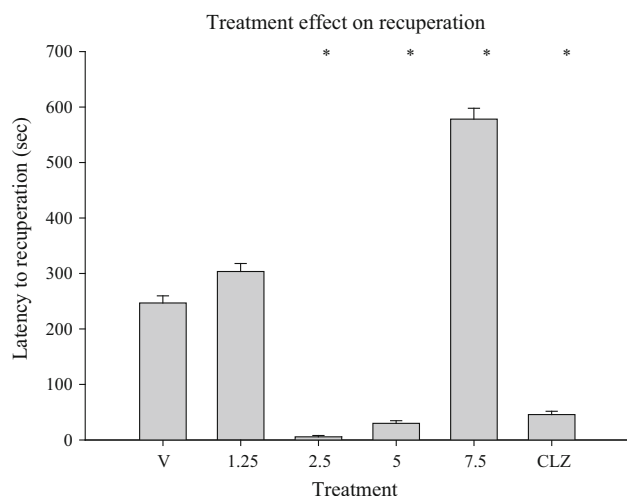


Fig. 6 Effect of D1 on the latency of the recuperation (in seconds) from the convulsions induced by PTZ in male rats. Each point represents the mean \pm CI for $n = 6$ rats per dose. *Significant effect compared with the V group (non-parametric one-way ANOVA, $p < 0.05$)

($\chi^2_{(0.05,5)} = 11,066$, $p < 0.05$). Treatment with D1 at 1.25 and 7.50 mg/kg resulted in a longer duration of the seizure than group V, CLZ, and D1 at 2.50 and 5.00 mg/kg ($\chi^2_{(0.05,5)} = 3,918.0$, $p < 0.05$). Finally, the recuperation variable showed that there was a significant difference between the three groups (CLZ and D1 using 2.50 and 5.00 mg/kg) and the other treatments ($\chi^2_{(0.05,5)} = 3,888.0$, $p < 0.05$) (Figs. 4, 5, 6).

In the PTZ-induced seizure model, a single CLZ administration (5.0 mg/kg) conferred protection by reducing the appearance and duration of seizures. A similar reduction in the duration of seizures was obtained with the two intermediate doses (2.50 and 5.00 mg/kg) of D1. On the other hand, the onset of the seizure was most delayed by D1 at 2.50 mg/kg. Thus, D1 at 2.50 mg/kg exerted the same effect as CLZ at 5.00 mg/kg. Considering molar equivalent doses, a CLZ dose of 5.0 mg/kg is equivalent to 15.83 $\mu\text{mol/kg}$, whereas a D1 dose of 2.50 mg/kg is equivalent to 10.05 $\mu\text{mol/kg}$. This demonstrates that the doses are not bioequivalent and that D1 has better efficacy (the same response at a lower dose in both weight and the number of administered molecules) [54, 55]. Contrary to the predictions from the dose–response curve, treatment with the higher concentration of D1 (7.50 mg/kg) did not show a biological effect, which is due to an effect called hormesis. The word “hormesis” originates from Greek, and means “arouse”. In a pharmacotoxicological context, hormesis describes substances that have a beneficial effect at low doses but cause a suppression effect at higher concentrations [56–59]. A hormetic effect produces a U or

inverted U curve, which is the case for D1. Test compounds with high biological activity show a hormetic effect, which is independent of the test or animal model [60]. Thus, we hypothesize that the hormetic behavior is mediated by a saturation of the GABAergic system, resulting in the suppression of the beneficial effect, but these processes should be further investigated. Finally, the 1,4 position of the two amine groups and the aromatics rings are fundamental to CNS activity; diazocines analogs with amines in the 1,6 positions and pyrazolic rings proved to be inactive in the CNS [61].

Conclusions

Our results show that compounds A–D, 1–25 have affinity for the GABA_AR. The compounds with the highest affinity for GABA_AR have binding sites and similar interactions to those of the four reference compounds (CLZ, ZOP, ESZ, and DZP). Therefore, these molecules may have properties similar to BZDs and act through a similar mechanism. Docking results indicate that carboxyl and amine functional groups in the *meta* and *para* positions result in greater affinity for amino acid residues. Another determining factor for affinity is molecular size. Compounds with a smaller ring size (i.e., BZD) than others (i.e., dibenzazepines) will have functional groups with more possibilities for interaction. The preliminary theoretical data suggests that D1 compound could be one candidate to be tested and also it was more straightforward to be synthesized. To corroborate the map of interactions observed through docking procedures, MD simulations were performed for the GABA_AR–D1 complex and also for the complex formed between GABA_AR and CLZ, ZOP or ESZ. Refined complex conformations were found for the GABA_AR–D1, GABA_AR–CLZ and GABA_AR–ZOP complexes and the two BZDs (D1 and CLZ) had similar maps of interactions and Gibbs free energies. The efficacy of D1 was evaluated as an anticonvulsant agent using a PTZ-induced seizure model. The anticonvulsant test showed that D1 possesses similar activity to CLZ, which is used as a treatment in seizure control and corroborates the predicted binding free energy of D1 that was determined through theoretical calculations.

Based on these results, it is clear that future studies should focus on the synthesis of related compounds that show greater theoretical affinity, with the goal of testing for possible activities as anticonvulsant, anti-anxiety, or sedative agents. Additionally, the toxicity of these compounds should be determined.

Acknowledgments We thank CONACYT (Grant: 132353), CYTED: 214RT0482 and SIP (project 20140252)-COFAA-PIFI/IPN for

financial support. Thanks to Cinthya Czajkowski Ph.D. (University of Wisconsin-Madison) for providing us with the GABA_AR coordinate. In memory of Dr. J. Samuel Cruz-Sánchez.

References

- Chebib M, Johnston GAR (1999) The ‘ABC’ of GABA receptors: a brief review. *Clin Exp Pharmacol Physiol* 26:937–940
- Khan ZU, Gutierrez A, De Blas AL (1994) The subunit composition of a GABA_A/benzodiazepine receptor from rat cerebellum. *J Neurochem* 63:371–374
- Hanson SM, Morlock EV, Satyshur KA, Czajkowski C (2008) Structural mechanisms underlying benzodiazepine modulation of the GABA_A receptor. *J Neurosci* 28:3490–3499
- Duncalfe LL, Dunn SM (1993) Benzodiazepine binding to GABA_A receptors: differential effects of sulphydryl modification. *Eur J Pharmacol* 246:141–148
- Sigel E (2002) Mapping of the benzodiazepine recognition site on GABA(A) receptors. *Curr Top Med Chem* 2:833–839
- Rowlett JK, Cook JM, Duke AN, Platt DN (2005) Selective antagonism of GABA_A receptor subtypes: an in vivo approach to exploring the therapeutic and side effects of benzodiazepine-type drugs. *CNS Spectr* 10:40–48
- Orser BA (2006) Extrasynaptic GABA_A receptors are critical targets for sedative-hypnotic drugs. *J Clin Sleep Med* 2:S12–S18
- Fonlupt P, Croset M, Lagarde M (1990) Benzodiazepine analogues inhibit arachidonate-induced aggregation and thromboxane synthesis in human platelets. *Br J Pharmacol* 101:920–924
- Migliaria O, Plescia S, Diana P, Di Stephano V, Camarda L, Dallolio R (2004) Synthesis and pharmacological evaluation of 7-substituted 1-ethyl-3,4,10-trimethyl-1,10-dihydro-11H-pyrazolo[3,4-c] [1,6]benzodiazocin-11-one: a new ring system. *ARKIVOC* V:44–53
- Koriatopoulou K, Karousis N, Varvounis G (2008) Novel synthesis of the pyrrolo[2,1-c][1,4]benzodiazocine ring system via a Dieckmann condensation. *Tetrahedron* 64:10009–10013
- Venkatachalan SP, Czajkowski C (2012) Structural link between γ -aminobutyric acid type A (GABA_A) receptor agonist binding site and inner β -sheet governs channel activation and allosteric drug modulation. *J Biol Chem* 287:6714–6724
- Morlock EV, Czajkowski C (2011) Different residues in the GABA_A receptor benzodiazepine binding pocket mediate benzodiazepine efficacy and binding. *Mol Pharmacol* 80:14–22
- Muroi Y, Czajkowski C, Jackson MB (2006) Local and global ligand-induced changes in the structure of the GABA(A) receptor. *Biochemistry* 45:7013–7022
- Xie HB, Sha Y, Wang J, Cheng MS (2013) Some insights into the binding mechanism of the GABA_A receptor: a combined docking and MM-GBSA study. *J Mol Model* 12:5489–5500
- Macías-Pérez ME, Martínez-Ramos F, Padilla-Martínez II, Correa-Basurto J, Kispert L, Mendieta-Wejebe JE, Rosales-Hernández MC (2013) Ethers and esters derived from apocynin avoid the interaction between p47phox and p22phox subunits of NADPH oxidase: evaluation in vitro and in silico. *Biosci Rep* 33:605–616. doi:10.1042/BSR20130029
- Bello M, Martínez-Archundia M, Correa-Basurto J (2013) Automated docking for novel drug discovery. *Expert Opin Drug Discov* 8:821–834
- Lipinski CA, Lombardo F, Dominy BW, Feeney PJ (2001) Experimental and computational approaches to estimate solubility and permeability in drug discovery and development settings. *Adv Drug Deliv Rev* 46(1–3):3–26
- Dalafave DS, Prisco G (2010) Inhibition of antiapoptotic BCL-XL, BCL-2, and MCL-1 proteins by small molecule mimetics. *Cancer Inform* 9:169–177
- Correa-Basurto J, Flores-Sandoval C, Marín-Cruz J, Rojo-Dominguez A, Espinoza-Fonseca LM, Trujillo-Ferrara JG (2007) Docking and quantum mechanic studies on cholinesterases and their inhibitors. *Eur J Med Chem* 42:10–19
- Kollman PA, Massova I, Reyes C, Kuhn B, Huo S, Chong L, Lee M, Lee T, Duan Y, Wang W, Donini O, Cieplak P, Srinivasan Y, Case DA, Cheatham TE III (2000) Calculating structures and free energies of complex molecules: combining molecular mechanics and continuum models. *Acc Chem Res* 33:889–897
- Miller BR, McGee TD, Swails JM, Homeyer N, Gohlke H, Roitberg AE (2012) MMPBSA.py: an efficient program for end-state free energy calculations. *J Chem Theory Comput* 8(9):3314–3321
- Munthe AW, Strandjord RE (1973) Clonazepam in the treatment of epileptic seizures. *Acta Neurol Scand Suppl* 53:97–102
- Martínez C, Rabadán FP, Galán J (1977) Modification of clonazepam anticonvulsive activity by its association with other anti-epileptic drugs. *Experientia* 33:640–642
- Stewart JJP (1989) Optimization of parameters for semiempirical methods I. Method. *J Comp Chem* 10(2):209–220
- Stewart JJP (1989) Optimization of parameters for semiempirical methods II. Applications. *J Comp Chem* 10:221–264
- Becke AD (1993) A new mixing of Hartree–Fock and local density-functional theories. *J Chem Phys* 98:1372
- Lee C, Yang W, Parr RG (1988) Development of the Colle–Salvetti correlation energy formula into a functional of the electron density. *Phys Rev B* 37:785–789
- Godbout N, Salahub D, Andzelm J, Wimmer E (1992) Optimization of Gaussian-type basis sets for local spin density functional calculations. Part I. Boron through neon, optimization technique and validation. *Can J Chem* 70:560–571
- Frisch MJ, Trucks GW, Schlegel HB, Scuseria GE, Robb MA, Cheeseman JR, Scalmani G, Barone V, Mennucci B, Petersson GA, Nakatsuji H, Caricato M, Li X, Hratchian HP, Izmaylov AF, Bloino J, Zheng G, Sonnenberg JL, Hada M, Ehara M, Toyota K, Fukuda R, Hasegawa J, Ishida M, Nakajima T, Honda Y, Kitao O, Nakai H, Vreven T, Montgomery JA Jr, Peralta JE, Ogliaro F, Bearpark M, Heyd JJ, Brothers E, Kudin KN, Staroverov VN, Kobayashi R, Normand J, Raghavachari K, Rendell A, Burant JC, Iyengar SS, Tomasi J, Cossi M, Rega N, Millam NJ, Klene M, Knox JE, Cross JB, Bakken V, Adamo C, Jaramillo J, Gomperts R, Stratmann RE, Yazyev O, Austin AJ, Cammi R, Pomelli C, Ochterski JW, Martin RL, Morokuma K, Zakrzewski VG, Voth GA, Salvador P, Dannenberg JJ, Dapprich S, Daniels AD, Farkas Ö, Foresman JB, Ortiz JV, Cioslowski J, Fox DJ, Gaussian, Inc. (2004) Gaussian 03, revision C.02. Gaussian, Inc., Wallingford, CT
- Morris GM, Goodsell DS, Halliday RS, Huey R, Hart WE, Belew RK, Olson AJ (1998) Automated docking using a Lamarckian genetic algorithm and an empirical binding free energy function. *J Comp Chem* 19:1639–1662
- Humphrey W, Dalke A, Schulten K (1996) VMD: visual molecular dynamics. *J Mol Graph* 14:33–38
- MacKerell AD, Bashford D, Bellott M, Dunbrack RL, Evanseck JD, Field MJ, Fischer S, Gao J, Guo H, Ha S, Joseph-McCarthy D, Kuchnir L, Kuczera K, Lau FTK, Mattos C, Michnick S, Ngo T, Nguyen DT, Prodhom B, Reiher WE, Roux B, Schlenkrich JC, Smith R, Stote J, Straub M, Watanabe J, Wirkiewicz-Kuczera DY, Karplus M (1998) All-atom empirical potential for molecular modeling and dynamics studies of proteins. *J Phys Chem B* 102:3586–3616
- Phillips JC, Braun R, Wang W, Gumbart J, Tajkhorshid E, Villa E, Chipot C, Skeel RD, Kalé L, Schulten K (2005) Scalable molecular dynamics with NAMD. *J Comput Chem* 26:1781–1802

34. Goodford PJ (1985) A computational procedure for determining energetically favourable binding sites on biologically important macromolecules. *J Med Chem* 28:849–857
35. Case DA, Babin V, Berryman JT, Betz RM, Cai Q, Cerutti DS, Cheatham TE III, Darden TA, Duke RE, Gohlke H, Goetz AW, Gusarov S, Homeyer N, Janowski P, Kaus J, Kolossváry I, Kovalenko A, Lee TS, LeGrand S, Luchko T, Luo R, Madej B, Merz KM, Paesani F, Roe DR, Roitberg A, Sagui C, Salomon-Ferrer R, Seabra G, Simmerling CL, Smith W, Swails J, Walker RC, Wang J, Wolf RM, Wu X, Kollman PA (2012) AMBER 12. University of California, San Francisco
36. Wang M, Cieplak P, Kollman PA (2000) How well does a restrained electrostatic potential (RESP) model perform in calculating conformational energies of organic and biological molecules? *J Comput Chem* 21:1049–1074
37. Wang J, Wolf RM, Caldwell JW, Kollman PA, Case DA (2004) Development and testing of a general Amber force field. *J Comput Chem* 25:1157–1173
38. Jakalian A, Jack DB, Bayly CI (2002) Fast, efficient generation of high-quality atomic charges. AM1-BCC model: II. Parameterization and validation. *J Comput Chem* 23:1623–1641
39. Jorgensen WL, Chandrasekhar J, Madura JD, Impey RW, Klein ML (1983) Comparison of simple potential functions for simulating liquid water. *J Chem Phys* 79:926–935
40. Van Gunsteren WF, Berendsen HJC (1997) Algorithm for macromolecular dynamics and constraint dynamics. *Mol Phys* 34:1311–1327
41. Darden T, York D, Pedersen L (1993) Particle mesh Ewald-an N.log(N) method for Ewald sums in large systems. *J Chem Phys* 98:10089–10092
42. Berendsen HJC, Postma JPM, Van Gunsteren WF, Di Nola A, Haak JR (1984) Molecular dynamics with coupling to an external bath. *J Chem Phys* 81:3684–3690
43. DeLano WL (2002) The PyMOL molecular graphics system, DeLano Scientific LLC, San Carlos, CA. <http://www.pymol.org>
44. Hawkins GD, Cramer CJ, Truhlar DG (1996) Parametrized models of aqueous free energies of solvation based on pairwise descreening of solute atomic charges from a dielectric medium. *J Phys Chem* 100:19824–19839
45. Kuhn B, Kollman PA (2000) Binding of a diverse set of ligands to avidin and streptavidin: an accurate quantitative prediction of their relative affinities by a combination of molecular mechanics and continuum solvent models. *J Med Chem* 43:3786–3791
46. Paudler WW, Zeiler AG (1969) Diazocine chemistry. V. Synthesis and rearrangement of dibenzo[b, f] [1, 4]diazocine-6,11(5H,12H)-dione. *J Org Chem* 34:2138–2140
47. Venugopalan B, Lyer SS, De Souza NJ (1985) TiCl₄-induced functionalization of dibenzo[b, f] [1, 4]diazocine-6,11-(5H,12H)-diones. *Heterocycles* 23:1425–1430
48. Marescaux C, Micheletti G, Vergnes M, Depaulis A, Rumbach L, Warter JM (1984) A model of chronic spontaneous petit mal-like seizures in the rat: comparison with pentylenetetrazol-induced seizures. *Epilepsia* 25:326–331
49. Schmoll H, Brandan I, Grecksch G, Walker L, Kessler C, Popa A (2003) Kindling status in Sprague-Dawley rats induced by pentylenetetrazole. *Am J Pathol* 162:1027–1034
50. López ML, González ME, Neri L, Hong E, Rocha LL (2005) 5-HT_{1A} receptor agonists modify epileptic seizures in three experimental models in rats. *Neuropharmacology* 49:367–375
51. Hanson SM, Morlock EV, Satyshur KA, Czajkowski C (2008) Structural requirements for eszopiclone and zolpidem binding to the GABA_A receptor are different. *J Med Chem* 51:7243–7252
52. Berezhnoy D, Gibbs TT, Farb DH (2009) Docking of 1,4-benzodiazepines in the alpha1/gamma2 GABA(A) receptor modulator site. *Mol Pharmacol* 76:440–450
53. Kim KS, Lee JY, Lee SJ, Ha T, Kim DH (1994) On binding forces between aromatic ring and quaternary ammonium compounds. *J Am Chem Soc* 116:7399–7400
54. Ehler FJ, Ragan J, Chen A, Roeske WR, Yamamura HI (1982) Modulation of benzodiazepine receptor binding: insight into pharmacological efficacy. *Eur J Pharmacol* 78:249–253
55. Morelli M, Gee KW, Yamamura HI (1982) The effect of GABA on in vitro binding of two novel non-benzodiazepines, PK 8165 and CGS 8216, to benzodiazepine receptors in the rat brain. *Life Sci* 31:77–81
56. Calabrese EJ, Baldwin LA (2003) Hormesis: the dose–response revolution. *Annu Rev Pharmacol Toxicol* 43:175–197
57. Riccia L, Valotia M, Sgaraglia G, Frosini M (2007) Neuroprotection afforded by diazepam against oxygen/glucose deprivation-induced injury in rat cortical brain slices. *Eur J Pharmacol* 561:80–84
58. Kouda K, Iki M (2010) Beneficial effects of mild stress (hermetic effects): dietary restriction and health. *J Physiol Anthropol* 29:127–132
59. Calabrese EJ (2010) Hormesis is central to toxicology, pharmacology and risk assessment. *Hum Exp Toxicol* 29:249–261
60. Calabrese EJ (2008) An assessment of anxiolytic drug screening tests: hormetic dose responses predominate. *Crit Rev Toxicol* 36:489–542
61. Miglaria O, Plescia S, Patrizia D, Di Stefano V, Camarda L, Dall’Olio R (2004) Synthesis and pharmacological evaluation of 7-substituted 1-ethyl-3,4,10-trimethyl-1,10-dihydro-11H-pyrazolo[3,4-c][1,6]benzodiazocin-11-one. A new ring system. *ARKIVOC*. V:44–53
62. Wallace AC, Laskowski RA, Thornton JM (1995) LIGPLOT: a program to generate schematic diagrams of protein–ligand interactions. *Protein Eng* 8:127–134